CoboSkin: Soft Robot Skin With Variable Stiffness for Safer Human–Robot Collaboration

Gaoyang Pang, *Student Member, IEEE*, Geng Yang, *Member, IEEE*, Wenzheng Heng, Zhiqiu Ye, Xiaoyan Huang, *Member, IEEE*, Hua-Yong Yang, and Zhibo Pang, *Senior Member, IEEE*

***Abstract*—Conventional industrial robots are unable to guarantee the inherent safety when working together with humans due to the use of rigid components and the lack of force sensation. To enhance the safety of human–robot collaboration (HRC), the new collaborative robot skin (CoboSkin) with the features of softness, variable stiffness, and sensitivity is designed and studied in this article. The CoboSkin is composed of an array of inflatable units and sensing units. The sensing units made of soft porous materials are capable of measuring distributed contact force in a real-time manner. By leveraging the foaming process, the sensing units are interconnected with inflatable units fabricated by the elastomer of which the deformation is limited by the textile wrapped around it. Variation of stiffness is enabled by adjusting the internal air pressure supplied to inflatable units, thereby changing the sensitivity of the sensing units and reducing the peak impact force. Soft porous materials endowed the CoboSkin with increased sensitivity, minimal hysteresis, excellent cycling stability, and response time in the millisecond range, which enabled sensing feedback for controlling a robot arm at different levels of stiffness. Finally, the validation of the CoboSkin for safer HRC was conducted with a robot arm to detect an unintended collision, illustrating its potential application in robotics.**

***Index Terms*—Human–robot collaboration (HRC), robot skin, safety, variable sensitivity, variable stiffness.**

I. Introduction

ADVANCEMENTS in human–robot collaboration (HRC) are expanding the applications of robots from the traditional production line to a more diverse range of scenarios, such as intelligent manufacturing [1], homecare [2], healthcare [3], aerospace [4], and education [5]. In particular, HRC has been recognized as an emerging technology of homecare robotics in Healthcare 4.0 [6]. One of the main challenges of HRC is that safety is not always guaranteed in collaborative robots (Cobots), as they are mainly made of rigid components that can cause serious injuries to humans during physical collisions [7], [8].

Most cobots adopt the compliant mechanisms and lightweight design to reduce the impact force once collisions occurred, such as ABB YuMi robot, but this is limiting their positioning accuracy and payload (0.5 kg per arm) [9], [10]. In addition to inherently structural design, several researchers have partly addressed the safety issue by leveraging one of power and force limiting (PFL) methods based on temporal dynamic models and current signals from embedded torque sensors [11]. However, the minimum detectable force of this method was relatively high, which may not match the demand for the maximum allowance force of the human body. Moreover, the spatial resolution of their method was inherently limited by the current signal. The combination of soft components and other safety improvement strategies improves robot safety performance, regarded as a typical solution for safety issues in current industrial robots for HRC [12], [13]. Comparing with the above methods, endowing cobots with the soft robot skin, of which the stiffness is self-adjusted along with the variation of working speed or together with active actuators, is a complementary way to increase the safety levels of cobots [14], [15]. Generally, stiffness varying methods can be classified into structure-based strategies and material-based strategies [16], [17]. Using airbags or soft foam to cover the robot's surface is an industrial practice to improve the safety performance of cobots. For example, YuMi robot is padded with soft foam materials to reduce the impairment to humans during a collision. As one of the structure-based strategies, stiffness controlled by air pressure is more compatible with this

Manuscript received August 9, 2019; revised November 28, 2019, January 21, 2020, and February 12, 2020; accepted February 23, 2020. Date of publication March 13, 2020; date of current version December 8, 2020. This work was supported in part by the National Natural Science Foundation of China under Grant 51975513, in part by the Major Research Plan of National Natural Science Foundation of China under Grant 51890884, in part by the Natural Science Foundation of Zhejiang Province, China under Grant LR20E050003, in part by the Zhejiang University Special Scientific Research Fund for COVID-19 Prevention and Control under Grant 2020XGZX017, in part by the Science Fund for Creative Research Groups of the National Natural Science Foundation of China under Grant 51821093, in part by the Robotics Institute of Zhejiang University under Grant K18-508116-008-03, and in part by the China's Thousand Talents Plan Young Professionals Program. *(Gaoyang Pang and Wenzheng Heng are co-first authors.) (Corresponding author: Geng Yang.)*

Gaoyang Pang, Geng Yang, Wenzheng Heng, Zhiqiu Ye, and Hua-Yong Yang are with the State Key Laboratory of Fluid Power and Mechatronic Systems, School of Mechanical Engineering, Zhejiang University, Hangzhou 310027, China (e-mail: gaoyangpang@zju.edu.cn; yanggeng@zju.edu.cn; 3160104443@zju.edu.cn; yezhiqiu1996@zju.edu.cn; yhy@zju.edu.cn).

Xiaoyan Huang is with the College of Electrical Engineering, Zhejiang Univerisity, Hangzhou 310027, China (e-mail: xiaoyanhuang@zju.edu.cn).

Zhibo Pang is with the ABB Corporate Research Sweden, 72178 Vasteras, Sweden (e-mail: pang.zhibo@se.abb.com).

This article has supplementary downloadable material available at http://ieeexplore.ieee.org.

Color versions of one or more of the figures in this article are available online at http://ieeexplore.ieee.org.

Digital Object Identifier 10.1109/TIE.2020.2978728

industrial practice. Therefore, soft robot skin with the capability of adjusting stiffness by using air pressure regulation is the desired solution to obtain safer HRC.

In HRC, efforts have been made to improve the cobot safety by developing various types of soft robot skins. To avoid dangerous contacts, Tsuji *et al.* [18] proposed a flexible robot skin for preventing collisions with humans using distance information between humans and robots collected by an array of time-of-flight sensors; Hughes *et al.* [19] described a flexible robot skin that composed of an array of optical proximity sensors embedded in a flexible material. In contrast to rigid commercially available proximity sensors, Matsuno *et al.* [20] presented a robot skin based on conductive fabric without affecting the stiffness of the robot link. The key challenges of these methods are the adaption of various curvatures of a robot body and mitigation impairment from collisions occurred by control or system errors. Therefore, the use of soft hyper-viscoelastic materials and cushion structure for constructing designated parts or entire robot skin becomes attractive because it can effectively reduce the impact forces and extend the energy transfer time. Yi *et al.* [21] proposed a soft inflatable robotic sleeve based on such methods for shock absorption. Ohta *et al.* [22] developed a robotic arm with the inflatable sleeves covering the rigid bone structure of it. Qi *et al.* [23] designed and implemented an interactive robot with lightweight inflatable arms. While the above examples improve the structural safety to some extent, most of them cannot directly and continuously provide external contact sensing and force feedback, which plays an important role in improving the responsiveness and autonomy of the robot [24]. To endow the robot skin with cushion and sensation simultaneously, Kim *et al.* [25] proposed a soft robot skin that had the inflatable structure with self-contained tactile sensing using microfluidic technology. The robot skin was capable of adjusting its stiffness by changing the internal air pressure. The robot skin was further improved for the increased safety of robots [26]. Although these approaches provide the soft robot skin with the sensing function, the initial impedance of sensing modules is affected by the inflation process. Furthermore, soft robot skin with a large volume design can interfere with the dynamic movements of the host robot.

In terms of commercially available soft robot skin, Papanastasiou *et al.* [37] utilized AirSkin Safety sensors (Blue Danube Robotics Inc.) designed with similar contours of host robots and wrapped with foam/rubber-based pads to enhance the collision detection functionality of HRC. However, the spatial resolution of this product is relatively large [28] and these sensors cannot locate the contact position precisely. Another safe robot skin—Smart Skin (FOGALE Robotics Inc.)—adopted the capacitive sensing method, enabling active avoidance of collision and detection of force's density. The skin also has limitations on the spatial resolution and cannot mitigate the impairment once a collision occurs since there is no cushioning component [29]. Combining a textile-based piezoresistive sensor array and a cushioning layer, a tactile sensor system (Fraunhofer IFF) enables the host robot to decelerate and stop in case of an unintentional collision to avoid high impact force to human counterparts [30]. Although the developed sensor system has a relatively high spatial resolution, the stiffness of the cushioning layer is unchangeable.

In this article, a safety improvement strategy for safer HRC is introduced, which is implemented based on a novel soft collaborative robot skin (CoboSkin) with the feature of variable stiffness and self-contained force sensing. The CoboSkin endows the cobot with the capability of reducing the collision force by adjusting the stiffness. In contrast to previous approaches, the proposed CoboSkin can avoid affecting the initial impedance of sensing units when altering the stiffness. In addition, it can also avoid affecting the dynamic movements of host robots when adjusting the stiffness. This article addresses the inherent design and implementation challenges with a detailed prototype design, manufacturing process, an exploratory CoboSkin characterization experiment, and experimental validation. This article has the following primary contributions and novelties: 1) a novel method for changing the stiffness of soft robot skin without the affecting the initial impedance of sensing units and the dynamic movements of host robots during the process of adjusting the stiffness; 2) a soft robot skin prototype (CoboSkin) with the feature of variable stiffness for the reduction of impact force during a collision and the modular design of the CoboSkin for its customized sensing function, stiffness, and dimensions to cover the cobot body; and 3) detailed manufacturing process, characterization, and experimental validation of the CoboSkin. To the best of our knowledge, this is the first approach combining multiple soft sensors into a robot skin through a foaming process.

II. Proposed Safety Improvement Strategy

A. Reduction of Impact Force With Variable Stiffness

From the results of prior works for constructing and analyzing the human–robot impact model, the stiffness of covering materials for the host robot is a key factor for the reduction of the impact force [31]. More importantly, there are related works based on these results in real application of HRC, such as inflatable sensing modules [25] and sleeves [26], indicating the feasibility of improving safety performance in HRC through variable stiffness. Thus, a safety improvement strategy based on the CoboSkin of which the stiffness can be changed is proposed in this article, as shown in Fig. 1. The CoboSkin is composed of an array of inflatable units and sensing units. The combination of one inflatable unit and one sensing unit is regarded as a functional module. The sensing units are capable of measuring distributed contact force. Variation of stiffness is enabled by adjusting the air pressure supplied to inflatable units of which the deformation is limited by the materials wrapped around it, thereby changing the sensitivity of the sensing units. In this article, the CoboSkin is developed and validated on the ABB YuMi robot [32].

B. Improvement of Host Robots Enabled by CoboSkin

Drawing upon the combination of the sensing unit and inflatable unit built on soft materials, CoboSkin is able to impact the ability of the host robot to interact with human peers in real-time. It is expected that the impact of proposed CoboSkin will be most effective in advancing the following robots' abilities: 1)

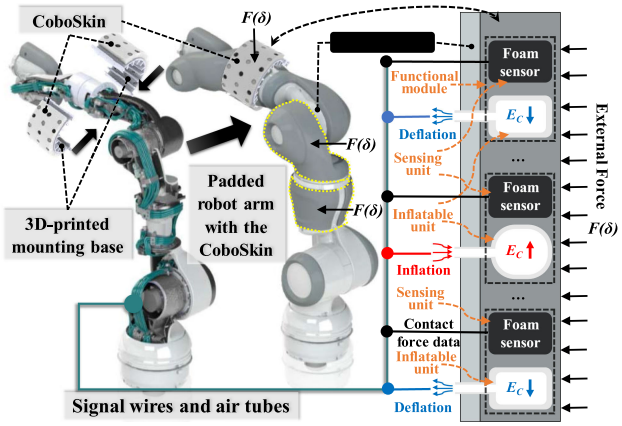

Fig. 1. Schematic illustration of the working principle of proposed safety improvement strategy, illustrated through the example of ABB YuMi robot [32]. E_c is the elastic modulus of covering materials.

TABLE I
SAFETY IMPROVEMENT STRATEGIES COMPARISON

Method	Contribution	Limitation
Lightweight design [32]	Reduction of M_R	Loss basic functionalities, reduction of overall performance, and limited coverage of safety issues
Compliant joint [33]	Adjustment of E_R	Non-immediately transient response to collision force, and extra mechanism at joint, leading to increased extra mass.
Compliant link [35]	Adjustment of E_R	Extra actuation is required.
Deformable component [25], [26]	Adjustment of E_C	Large volume deformation, leading to the interference with the sensing feedback and the dynamic movements of the robot.
CoboSkin (This work)	Adjustment of E_C	Extra fluid power supply for changing of the stiffness and complex modeling of sensing and stiffness.

Safety Assurance Ability—the possibility of designing bodies with intrinsic controllable stiffness to immediately respond to and reduce collision force, according to the parameters from dynamic environments, for the minimization of the impairment to human at the beginning of collision, such as high working speed with high stiffness and low working speed with low stiffness; and 2) Human-Robot Interaction Capability—the possibility of providing conventional cobots with a touch communication tool where the sensitivity is variable, such as high stiffness with low sensitivity and low stiffness with high sensitivity, enabling host robots with high-sensitivity detection of the user's touch when the working speed of host robot is low.

C. Comparison of Safety Improvement Strategies

In addition to the proposed strategy, there are several other reactive methods (i.e., the methods effected before the collision are defined as proactive methods; the methods effected after the collision are defined as reactive methods) for minimizing the injury caused by unintended collision, such as lightweight [32], compliant joint [33], [34], compliant link [35], and deformable component [26]. Their contribution and limitation are summarized in Table I, where E_R is the elastic modulus of robots and M_R is the mass of robots. Compared with the methods, the proposed strategy shows the advanced features, including minimum extra mass due to the lightweight soft porous materials and constant geometry dimensions, leading to the minimum interference with the dynamic movements of the host robot. Additionally, the process of changing stiffness does not affect the initial impedance of sensing units in CoboSkin, i.e., there is no offset of sensing output when the stiffness is changed. The feature of variable stiffness extends the linear sensing range and sensitivity.

D. Safety Standards of Human Pain Tolerance

The general standard for the safety of industrial robots has been given by the International Organization for Standardization (ISO) in EN ISO 10218 [36]. With the revolution from conventional robots to cobots, a new technical specification (TS), called ISO/TS 15066, as a supplement to EN ISO 10218 for safety issues, was published. In ISO/TS 15066, a collaborative operation related to this article is PFL where the risk reduction is achieved, either through inherently safe measures (e.g., means in Table I) in cobots or through a safety-related control system [8]. The standard describes the risk assessment of two approaches based on human pain tolerance in two aspects. One is based on allowable impact force [37], where the minimum tolerable force of face and neck are 90 and 35 N, respectively. Another is based on tolerable impact pressure [38], where the minimum permissible impact pressure of face and neck is 50 N/cm^2. The CoboSkin can be used to monitor these thresholds and make full use of its distinguishing features to improve the safety levels of host robots.

III. COBOSKIN

A. Structure Design

The structure of the CoboSkin and mounting methods on YuMi robot are demonstrated in Fig. 2, consisting of an array of inflatable units and sensing units. The combination of an inflatable unit and a sensing unit is regarded as one basic module of the CoboSkin, named as a functional module. Modularized designing is not only beneficial to reconfigure the numbers and distribution of modules, but also change the dimension of the CoboSkin. Polyurethane (PU) foam, as a soft porous material, is adopted for fabricating the carrier of the cylindrical sensing unit. Carbon black (CB), as a conductive nanomaterial, is deposited to the inner surface of the PU foam to form conductive backbones. The pressure-sensing mechanism is based on the conductive backbones (See Subsection C of Section III). The inflatable unit is made of silicon rubber (Ecoflex 00-30, Smooth-On, Macungie, PA, USA) with a structure of the cylindrical cavity. There is a pneumatic port that is connected to an air tube on the bottom of the inflatable unit. Each inflatable unit has a thickness of 1 mm. The height and diameter of the inflatable unit are 10 mm, which are equal to the sensing unit. Sensing units and inflatable units

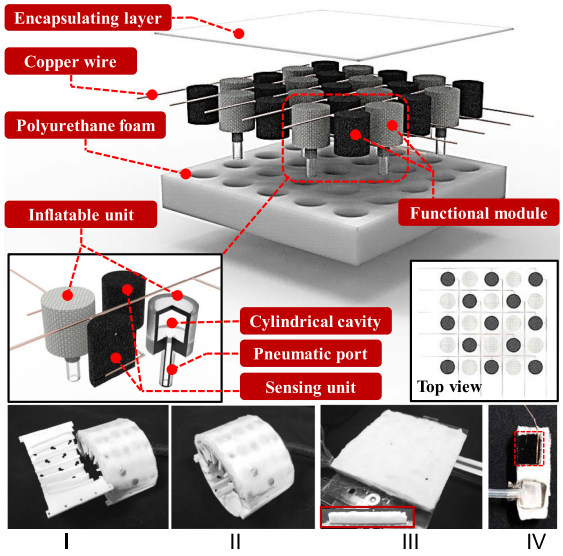

Fig. 2. Schematic illustration of the structure design of the CoboSkin. I. The photograph of the CoboSkin for YuMi robot before assembling. II. The photograph of the CoboSkin for YuMi robot after assembling. III. The photograph of flat CoboSkin for letter imaging. IV. The photograph of cross-sectional view of a single functional module.

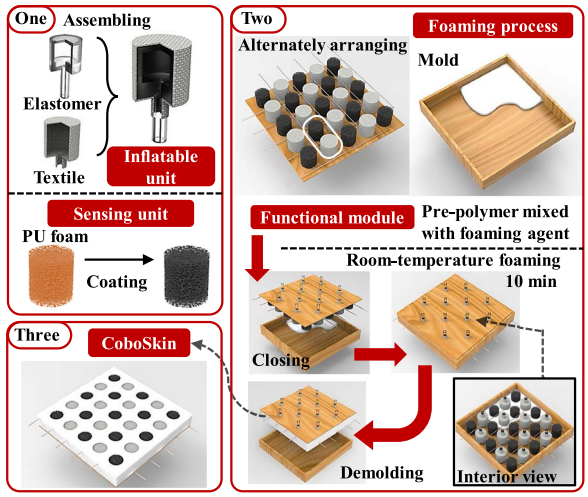

Fig. 3. Schematic illustration of fabrication steps of the CoboSkin.

are alternately arranged in the CoboSkin. The center distance of two adjacent units is 15 mm, indicating that the spatial resolution of force sensing is 30 mm. Even if the sensing unit and inflatable unit are side-by-side, the effects on the initial impedance of sensing units are still negligible to some extent (See Subsection B of Section IV). The soft material, as the base material of the entire CoboSkin, for interconnecting the sensing units and inflatable units is made by PU foam (FlexFoam-iT III, Smooth-On). As one limitation of this design, dead zones are detected above the inflatable units, which may be addressed by putting the sensing units inside the inflatable units in the future design.

B. Fabrication

The fabrication steps are illustrated in Fig. 3. To fabricate the sensing unit, the commercially available PU foam is cut with a laser machine according to the designed shapes. The cylindrical PU foam is then dip-coated with the uniformly mixed solvent that consists of CB and n-hexane, allowing it to be completely soaked. The coated PU foam is dried at a heating plate to deposit the CB into the porous material and remove the n-hexane naturally. To obtain stable measurements, two copper needles (length: 8 mm; diameter: 0.5 mm) are manually inserted into each sponge sensor unit. The copper needles embedded into adjacent sensor units are connected by enameled copper wires (diameter: 0.1 mm) through a soldering method. The enameled copper wires were deployed at the gap between the sensors and air chambers, forming a sensing matrix. Since the safety performance of reducing peak impact force depends on the feature of variable stiffness enabled only by inflatable units, there is no direct impact of individual difference induced by manual fabrication of sensing units on safety performance. The inflatable unit mainly consists of a structured elastomer with a cylindrical cavity and a nylon textile (thickness: 0.1 mm) wrapped around the elastomer by using a nylon cable tie. The elastomer is manufactured through a molding method. The prepolymer of silicon rubber is first mixed with the curing agent at a weight ratio of 1:1. The mixed solvent is poured into the 3-D printed mold designed for each part of the inflatable unit, vacuuming for five minutes and curing at room temperature. All the parts of the inflatable unit are assembled by silicone rubber adhesive. The prepared sensing units and inflatable units are alternately placed in a mold for the foaming process lasting for ten minutes at room temperature. After demolding, all the units are connected in the form of square arrays and form an entirety, that is, the modularized CoboSkin. It should be noted that the molds in the foaming process are wrapped around a layer of plastic film for easy demolding. By leveraging this fabrication method, the CoboSkin can also be further manufactured and mounted on the end-effector of cobots, which is regarded as the source of major safety hazard [39]. The mass of a single functional module without the air tube and enameled wires is 1.3 g, where the mass of embedded sponge sensor is 0.04 g, and the mass of embedded inflatable unit is 0.9 g. The mass of other parts, such as inserted copper wires and filled PU foam, is about 0.3–0.4 g.

C. Sensing Principle

The pressure-sensing mechanism of foam sensors is common [40]. As shown in Fig. 4, two main factors impact the resistance of the foam sensor when the sensor is loaded with an external force. One is the emerging microcracks at the weakest position, leading to a decrease of conductivity. Another is the contact of backbones, which is emerged with a higher load, resulting in an increasing number of conductive paths, thereby obviously rising the conductivity of the foam sensor. These two mechanisms both work at the initial stage of loading. Once the deformation of foam sensors reaches a certain degree, the later mechanism becomes to play a major role in the dropping trend of resistance. Thus,

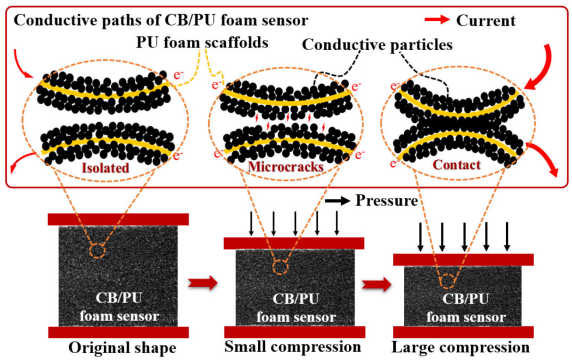

Fig. 4. Sensing principle of foam sensors.

the variation of sensors' resistance is reflected with an external contact force.

IV. Characterization and Validation

A. Characterization of the Modules

To characterize the basic performance of the module, an experimental setup was prepared (See more details in supplementary materials, Fig. S1). The functional module was experimentally characterized by supplying seven internal air pressure levels (0, 50, 100, 150, 200, 250, and 300 kPa). Fig. 5(a) and (b) illustrates the features of variable stiffness (k, which is defined by Δ Force/Δ Deformation) and force hysteresis of the functional module, which remained the linear elastic property of inflatable unit. As the internal air pressure increased from 0 to 300 kPa, the stiffness (k) of the functional module also rose steadily from 0.53 to 2.06 N/mm. Moreover, as shown in Fig. 5(b), when the internal air pressure increased, the force hysteresis of the functional module tended to decrease from 0.4 N (5% of full force range) to 0.35 N (4.37% of full force range). The force-deformation hysteresis is inherently induced by the viscoelastic material of the CoboSkin, including PU foam and silicon rubber [41]. The air in the inflatable unit exhibits elastic behavior, impacting the overall elastic behavior of the functional module. Increased internal air pressure leads to an increase in the elastic behavior of the functional module, thereby reducing the impact of viscoelastic material on viscoelastic behavior and resulting in a decrease in the hysteresis. Fig. 5(c) and (d) illustrates the calibration and sensing hysteresis of the functional module. When the functional module was loaded with increasing external force (0–10 N), the percentage change in impedance (PCI, the decrement of impedance divides the initial impedance of the sensing unit) decreased. The initial impedance is calculated by averaging the impedance value collected by a digital multimeter at a sampling rate of 50 Hz for about 15 s when the sensor is unloaded. Although the sensitivity (S, defined as Δ PCI/Δ Force) of the module was decreased from -25 to -6.1% with increased stiffness, the linear detection range was expanded from 1–3 to 4–10 N. Moreover, the sensing hysteresis of the functional module was reduced from 15.5% (19.4% of full sensing outputs) to 1.6% (2% of full sensing outputs) by increasing the internal air pressure, as illustrated in Fig. 5(c). As the internal air pressure increased, the sensing hysteresis of the functional module presented a similar tendency with force hysteresis. The results in Fig. 5(e) shows the reproducibility of the functional module that was loaded with a constant force of 5 N during the cyclic variation of internal air supply (0–100, 0–200, and 0–300 kPa). Fig. 5(f) shows the reproducibility of the functional module that was loaded with a cyclic external force from 0 to 5 N under seven internal pressure levels (0, 50, 100, 150, 200, 250, and 300 kPa). The results in Fig. 5(e) and (f) presents that the PCI of the functional module increased with the decreased internal air pressure while maintaining a stable initial impedance during each experiment that is validated by the repeated PCI of 0%. But it should be noticed that the initial impedance varied with different experiments that were conducted with a time interval of several days. The initial impedance of the same functional module being tested in Fig. 5(c)–(f) were about 2608, 2680, 2720, and 2643 Ω, respectively. This variability of initial impedance may be induced by the variation of experimental conditions, such as temperature and humidity. To reduce the influence of the variation of experimental conditions on initial impedance, a reference module (i.e., another functional module with the identical characteristics as the functional module being tested) can be introduced during the experiments in future work.

In addition to the characteristics mentioned above, the minimum detectable force of a single functional module was 0.1 N, as shown in Fig. 6(a). Since the impedance of the sensing unit is solely dependent on the deformation of the sensing unit, a calibration test of the percentage change in impedance with respect to the compressive deformation of the functional module was conducted, as shown in Fig. 6(b). The test sample used in Fig. 6(a) and (b) was the same one with Fig. 5(c)–(f), of which the initial impedance was about 2620 and 2700 Ω, respectively. To estimate the stiffness of the functional module in the full continuous range of the internal air pressure, the data in Fig. 5(a) were further fitted with a mathematical model, as illustrated in Fig. 6(c). Taking the influence of the inflation process on the initial impedance of the functional module into consideration, a comparison test of sensing response between the sample applied in this paper (AIP) and the sample with high spatial resolution design (HSRD, the distance between sensing unit and the inflatable unit is zero) was carried out. As illustrated in Fig. 7, the two samples were tested under the cyclic pressure regulation (0–100, 0–200, and 0–300 kPa) without loading external force. Since this comparison test aims to quantify the fluctuation induced by the inflation process, the baseline drift of the raw data was removed. The maximum fluctuation of the AIP is 0.01%, which is lower than that of the HSRD (0.15% with a cyclic pressure regulation of 0–300 kPa).

B. Characterization of Safety Performance

To evaluate the safety performance of the functional module, an experimental setup for collision testing was prepared to record the impact force [See more details in supplementary materials, Fig. S2]. As shown in Fig. 8(a) and (b), seven impact tests were conducted with different inflation pressure levels (0, 50, 100,

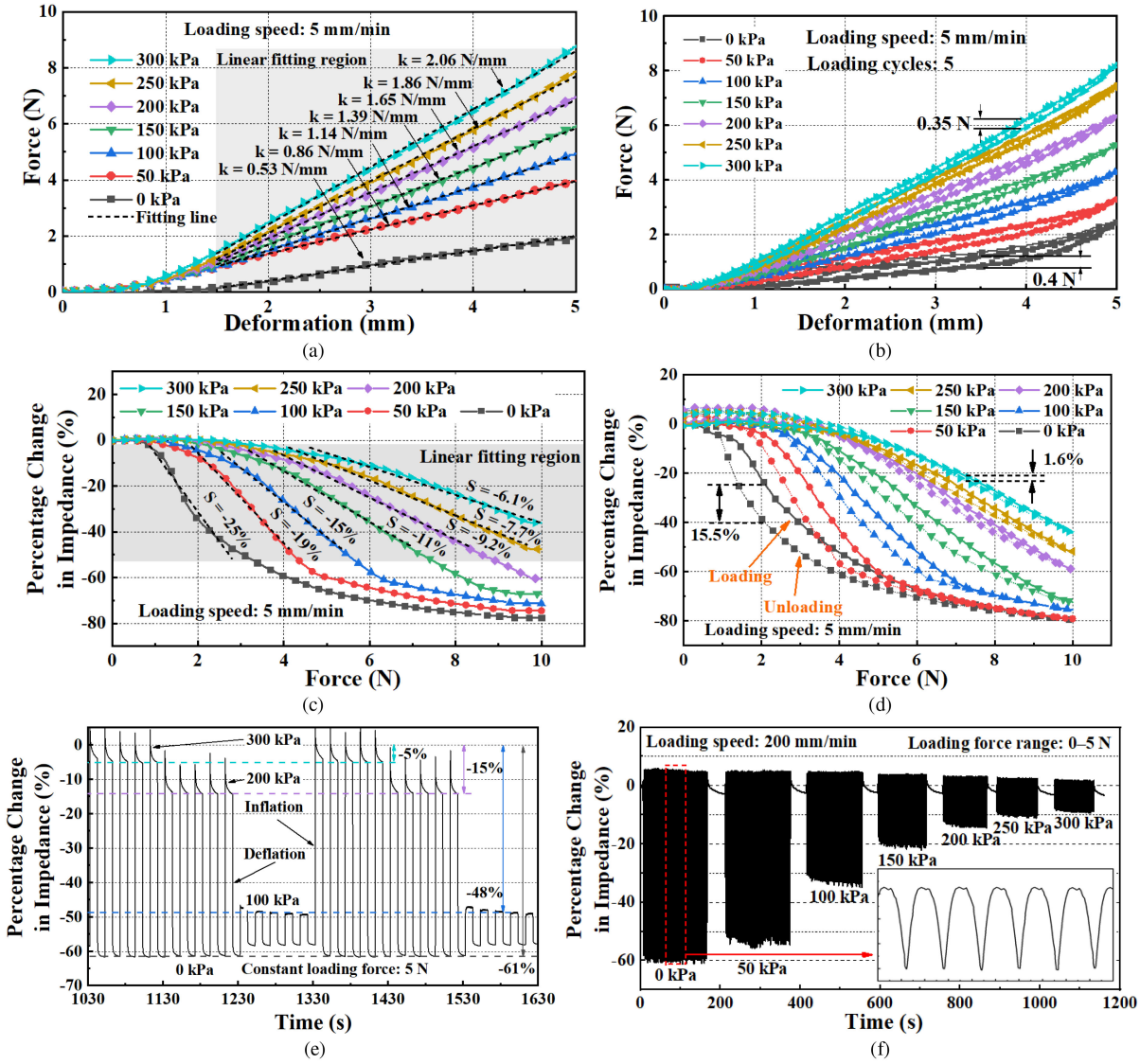

Fig. 5. Characterization of the functional module. (a) Calibration of variable stiffness of the functional module with seven internal pressure levels. (b) Force hysteresis of the functional module with seven pressure levels. (c) Calibration of variable sensitivity of the functional module with seven internal pressure levels. (d) Sensing hysteresis of the functional module with seven internal pressure levels. (e) Sensing response of functional module loaded with a constant force during the cyclic variation of internal air supply. (f) Sensing response of functional module loaded with a cyclic external force under seven internal pressure levels. The illustration in (f) is the part of reproducibility result ranged from 90 to 110 s.

150, 200, 250, and 300 kPa). The mass and speed of impact actuation were 1.426 kg and 0.83 m/s, respectively. Fig. 8(a) shows that the peak impact force tended to decrease from 93.26 to 69.10 N (a reduction of 25.9%) with the increased internal air pressure from 0 to 300 kPa. However, the degree of decrement of the peak impact force also decreased since the stiffness of the CoboSkin became higher at larger internal air pressure levels, despite the impulses of seven tests were in the same level (1.2 N·s). Through extending the energy transfer time, the peak impact force was reduced by the CoboSkin. As demonstrated in Fig. 8(b), the response time of the functional module is about 200 ms when the functional module was inflated with different internal air pressure. The results in Fig. 8(c) show that the work during the large compression of the functional module increased with internal air pressure. The compression process can be divided into two regions in terms of deformation (from 0–7 mm and from 7–8.5 mm). In the initial small compression, the curves illustrated a similar relationship with the results in Fig. 5(a). In the later large compression, almost all the curves showed a similar trend because the inflatable unit has been completely compressed. However, the overall transferred energy of two regions in each pressure level rose steadily from 0.59 to 1.02 J with increased stiffness, which means that the functional module had the potential to decrease initial impact velocity (i.e., the operation speed of robot) if the cushioning distance of CoboSkin and the effective mass of human and robot were constant. The more energy the functional module transfers, the larger the impact velocity CoboSkin could withstand during the collision. To quantify the ability to decrease/increase safe operation speed, the experiment has been conducted with three

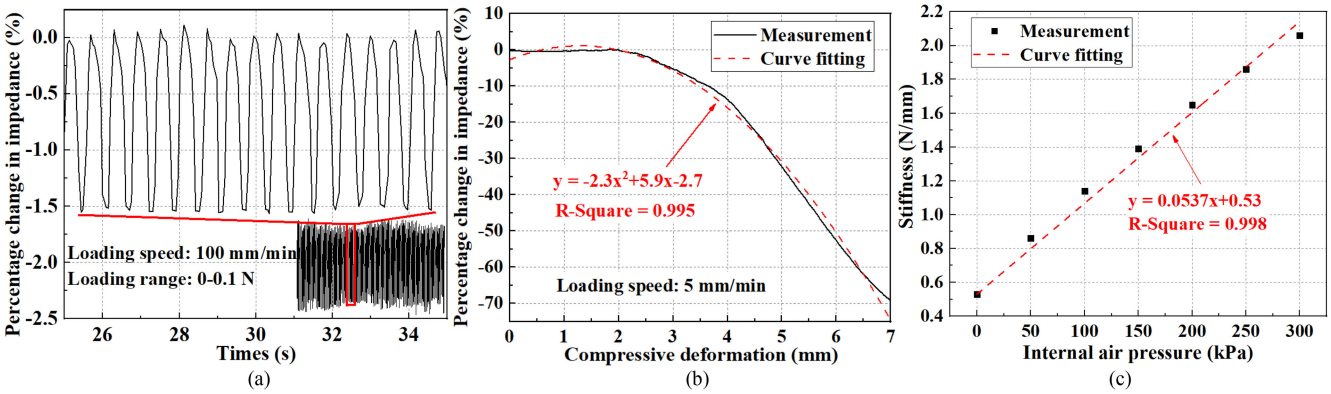

Fig. 6. Characterization of the functional module. (a) Reproducibility of the functional module with a loading force range of 0–0.1 N. (b) Mathematical model of PCI with respect to compressive deformation. (c) Mathematical model of the module stiffness with respect to internal air pressure.

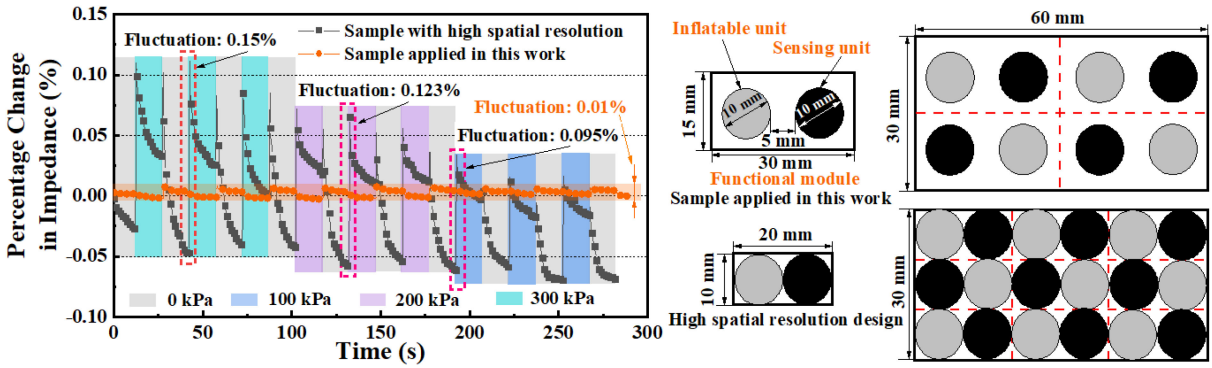

Fig. 7. Comparison of sensing response between the sample applied in this work and the sample with high spatial resolution design without loading external force during the cyclic inflation and deflation.

constant peak impact force levels to explore the relationship between the tolerable impact velocity and the internal air pressure, as shown in Fig. 8(d). In other words, every point in the plot refers to the maximum impact velocity with the constant peak impact force under the current stiffness. For the impact force level of 69 and 93 N, the internal air pressure could be increased to raise the tolerable impact velocity from 0.707 to 0.81 m/s and from 0.829 to 0.955 m/s, respectively. For an impact force level of 30 N, the internal air pressure should decrease from 300 to 50 kPa and the tolerable impact velocity will rise from 0.143 to 0.276 m/s. The maximum cushioning distance of CoboSkin is an important factor to induce the opposite tendency mentioned above. Compared with 69 and 93 N, the peak impact force of 30 N is relatively low and cannot result in the skin's compressive deformation that reaches to the maximum cushioning distance in an internal air pressure range from 50 to 300 kPa. In such a situation, it will be easier for the collision event to reach a higher peak impact force if the skin is stiffer. The skin should be softer to extend the cushioning distance to the maximum value, increasing the tolerable impact velocity while maintaining the tolerable impact force. If the skin is in an internal air pressure range from 0 to 50 kPa, the skin is too soft to absorb all impact energy, leading to the collision between human and robot's surface with a high peak impact force. The skin should be stiffer to absorb more impact energy, increasing the maximum tolerable impact velocity while maintaining the peak impact force. Therefore, to improve the safety assurance ability of the host robot, soft robot skin should equip with the function of altering stiffness when being involved in an unintended collision in dynamic environments.

C. Data Collection of CoboSkin

To collect the sensing data of the CoboSkin, a readout circuit based on the equipotential shielding method was designed and fabricated, which is controlled by a microcontroller (Arduino UNO). By leveraging voltage divider rule, the readout voltage sampled from the readout circuit defines the resistance variation of the sensing unit being tested without the bypass crosstalk [42]. The impedance data from the readout circuit are packaged and transferred by the Arduino and sent to a computer through the serial interface for real-time display of impedance change of the sensing unit being tested. The control signal triggered by the CoboSkin is sent to the same microcontroller that is connected to the XS8 DI port of YuMi robot's controller to trigger an interrupt signal for the robot during a collision [43]. Since the sensitivity of each sensing unit differs depending on the location of inserted

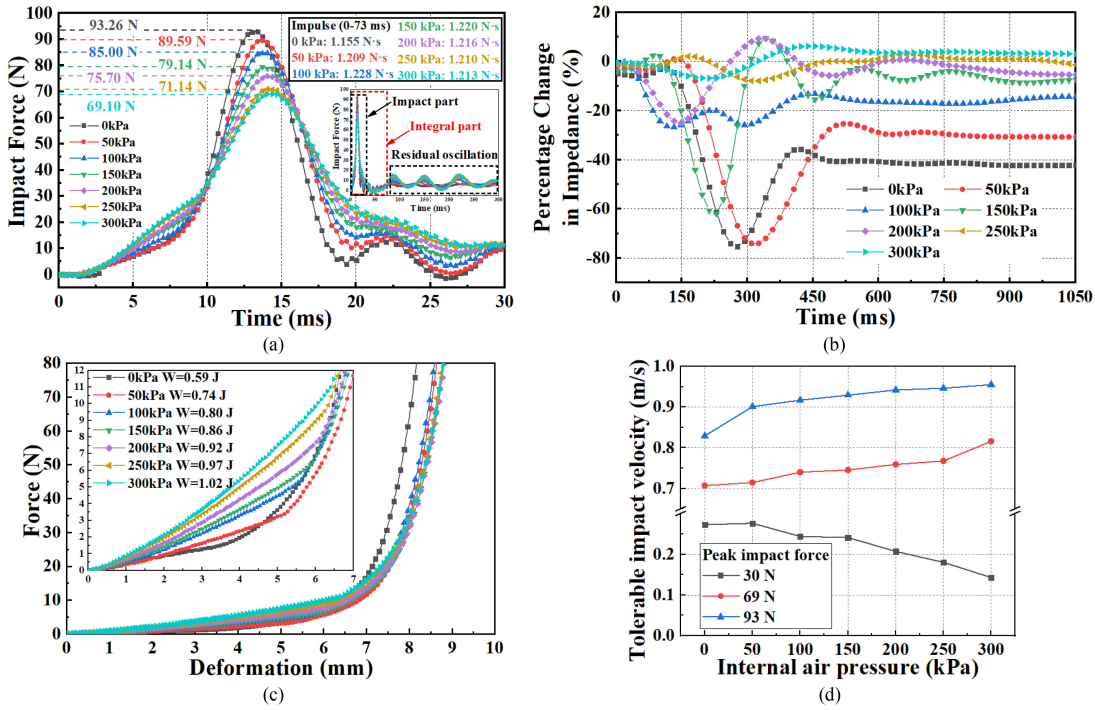

Fig. 8. Safety related performance of functional module. (a) Comparison of peak force and impulse with seven internal pressure levels. (b) Transient sensing response of functional module supplied with seven internal pressure levels. (c) Large compression response with seven levels of stiffness. (d) Reduction or increase of safe operation speed for cobots.

copper wires, a different amplification gain was applied to each sensing unit.

D. Validation of Sensing Response

To verify the function of the developed CoboSkin, the sensing response tests were carried out, including validation of variable sensitivity and stiffness, distributed contact force sensation, and the real-time data acquisition. The developed CoboSkin was composed of an array of sensing units, which were distributed in the form of a 3×3 matrix and a 4×4 matrix. The inflatable units were alternatively arranged among the sensing units. The total length and width of the CoboSkin are 110 mm, respectively, whereas the thickness is 10 mm. The sensing response of the CoboSkin is shown in Fig. 9. After placing of letters ("Z," "J," and "U"), the resistance of functional modules in the CoboSkin was first initialized to zero. The CoboSkin was then loaded with a weight of 10 kg. The weight was placed on a transparent plate above the letters for steady loading. All the functional modules in the CoboSkin were supplied with the same internal pressure level ranged from 0 to 100 kPa. The color of the squares in each picture indicates the decrement in the resistance value of each functional module during the cyclic inflation–deflation process at a frequency of 0.167 Hz. The decrement in the resistance value of the corresponding functional module changed significantly when it was inflated or deflated.

E. Validation of Safe Collaboration

A comparison of collision detection between the CoboSkin and the self-integrated collision detection module of YuMi robot is illustrated in Fig. 10. The CoboSkin was integrated onto the surface of YuMi robot through the 3-D printed mold method, as shown in Fig. 10(a). The developed CoboSkin composed of an array of sensing units, which were distributed in the form of a 3×4 matrix, and a 2×3 matrix. The inflatable units were alternatively arranged among the sensing units. The basswood laminated was selected as an obstacle for generating a collision force by using the robot link to bend it. Assuming that the judgment of a collision was a PCI from -18 to -22%, the contact force at different internal air pressure levels was showcased by the bending angles of basswood laminated. The speed of the tool center point (TCP) of the end-effector was set at 100 mm/s, respectively. Fig. 10(b) and (c) shows that using the larger internal air pressure (200 kPa) for the CoboSkin induced a larger bending angle (7.6°) of basswood laminated than that (6.9°) without inflation (0 kPa), which means that the sensitivity of the CoboSkin was varied with stiffness. For more clear demonstration, an amplification gain of five was applied to all the illustrations of contact force data (3-D color bar) in Fig. 10(b) and (c). Compared with Fig. 10(d), where the cobot exceeding the stroke (35.8°) without detection of a collision, the CoboSkin showed the capability to detect the low collision force. Combining this capability and the feature of reduction of peak force during a collision, the CoboSkin enables safer HRC. During the experiment, the magnitudes of different force levels were 16.6 N for 6.9°, 19.8 N for 7.6°, and 24 N for 35.8° at almost the same contact position when integrated with CoboSkin, and 39 N for 35.8° at exceeding contact position. In addition to the performance mentioned above, an experiment has been conducted to quantify the minimum detectable force of YuMi robot, of which the robot arm impacted the impact force sensor at different speeds of TCP and different sensitivity of

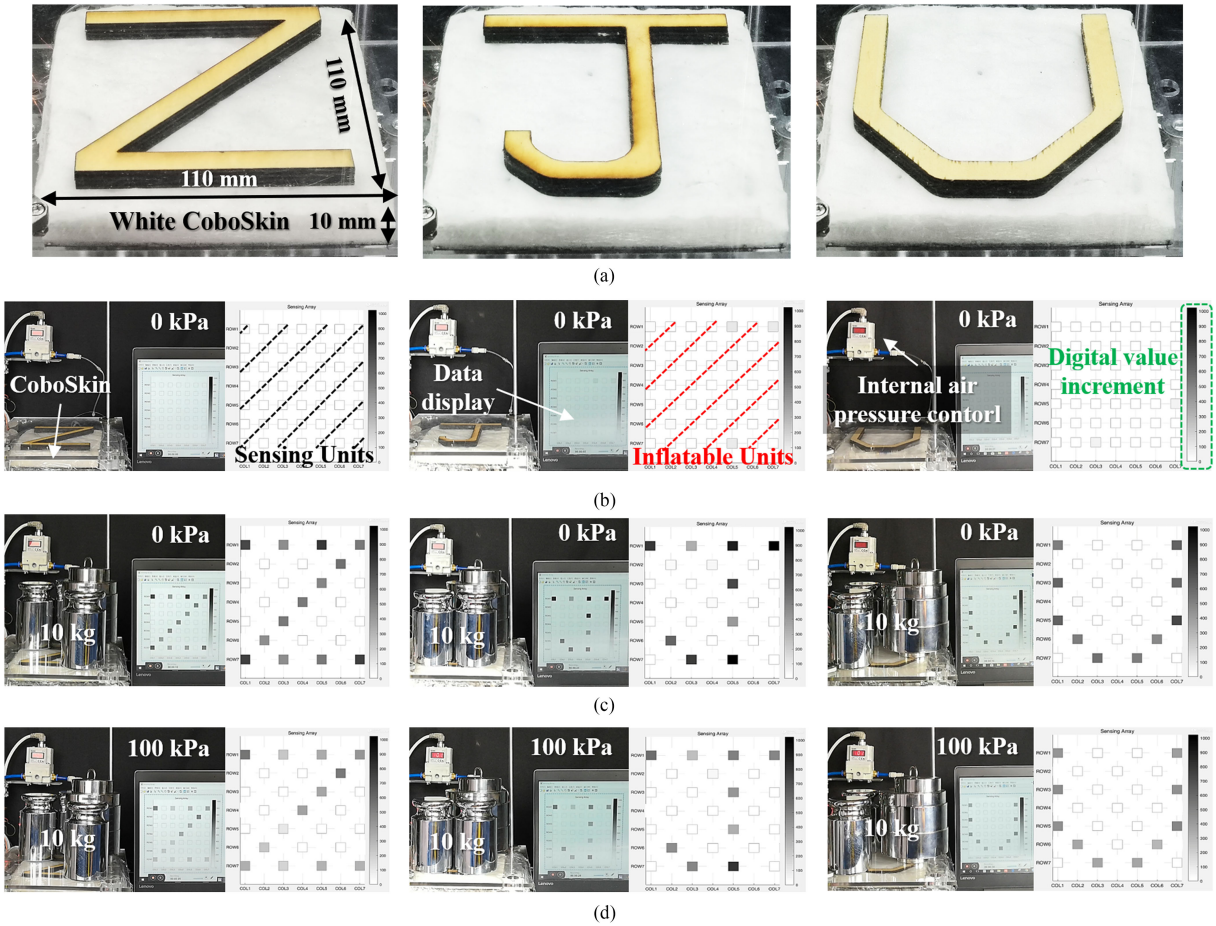

Fig. 9. Sensing response of the CoboSkin. (a) Loading force contact pattern composed of the letters such as "Z," "J," and "U." (b) Sensing response of the CoboSkin without external loading and inflation. (c) Sensing response of the CoboSkin being loaded with a weight of 10 kg without inflation. (d) The distributed sensing response of the CoboSkin being loaded with a weight of 10 kg and inflated with an internal pressure level of 100 kPa. Images are taken from a video sequence.

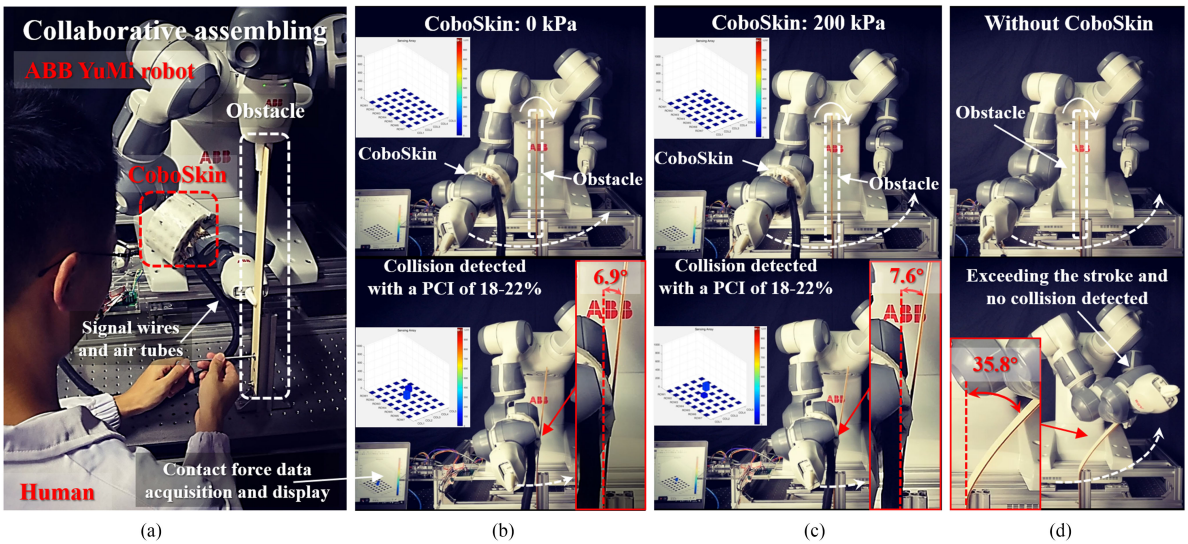

Fig. 10. Comparison of collision detection between the CoboSkin and the commercially available cobot without integrating the CoboSkin. (a) An overview of the CoboSkin prototype integrated on a dual-arm cobot, ABB YuMi robot, for safer human-robot collaboration in a collaborative assembling scenario. (b) Collision detection enabled by the CoboSkin without inflation. (c) Collision detection enabled by the CoboSkin with an internal air pressure level of 200 kPa. (d) Comparison of the self-integrated collision detection module of ABB YuMi robot. The module is enabled by the abnormal torque detected form each joint. Images are taken from a video sequence.

self-integrated collision detection module. The results indicated that the robot had a relatively higher minimum detectable force (5.125 N) than that of CoboSkin (0.1 N). Therefore, compared with YuMi robot, the developed CoboSkin were able to provide host robot with a much lower detectable force to enhance the safety performance.

V. Conclusion

In this article, a safety improvement strategy for safer HRC based on the CoboSkin was proposed. The CoboSkin was feasible for reducing the impact force during a collision by adjusting its internal air pressure. The CoboSkin increased the linear sensing and force detection range by increasing its internal air pressure level. Moreover, the force hysteresis and sensing hysteresis were reduced by increasing the internal air pressure level. The CoboSkin showed the excellent cycling stability during inflating the internal air pressure and loading external force, as well as the response time in the millisecond range. The proposed CoboSkin effectively avoided affecting the contact force sensing (a maximum fluctuation of 0.01%) and geometric structure during the process of adjusting the stiffness. Compared with the commercially available cobot, the CoboSkin had the capability of detection of low collision force and reduction of peak collision force.

In future work, the rectangular shape of basic units would be further investigated to fill the skin more evenly. The spatial resolution of the CoboSkin would be further increased by optimizing the structure design. The force-deformation hysteresis would be modeled by leveraging deep learning methods [44]. Since the tolerance capacity of the peak impact force of the CoboSkin was dependent on the inflatable unit, the optimization of the inflatable unit will be conducted especially in structure design and fabrication. For example, adopting materials with higher strength [45] and utilizing 3-D printing technology [46] were some practical solutions. To realize the advanced safe function of HRC, a control system for internal air supply would be developed and integrated with the CoboSkin for changing the stiffness along with the variation of working speed. To incorporate the CoboSkin to host robot and perform real-time trajectory planning for potential application in teleoperation as human-robot interfaces, the current robot's dynamic models and the corresponding collision matrix need to be further modified through redefining the armload according to the CoboSkin's model [47], [48]. Furthermore, the CoboSkin would be fabricated by exploiting 3-D printing technology to cover the complex contours of the entire robot body for increased safety with an active defense like humans. With the increasing number of the functional modules, to simplify the calibration process, an efficient way to make the sensitivities of all the sensing units same and to find the location of each skin patch as well as to manage tactile data would also be explored [49], [50].

References

[1] A. Cencen, J. C. Verlinden, and J. M. P. Geraedts, "Design methodology to improve human-robot coproduction in small- and medium-sized enterprises," *IEEE/ASME Trans. Mechatronics*, vol. 23, no. 3, pp. 1092–1102, Jun. 2018.

[2] D. Fischinger *et al.*, "Hobbit, a care robot supporting independent living at home: First prototype and lessons learned," *Robot. Auton. Syst.*, vol. 75, pp. 60–78, Oct. 2016.

[3] Z. Erickson, M. Collier, A. Kapusta, and C. C. Kemp, "Tracking human pose during robot-assisted dressing using single-axis capacitive proximity sensing," *IEEE Robot. Autom. Lett.*, vol. 3, no. 3, pp. 2245–2252, Jul. 2018.

[4] C.-Y. Weng, Q. Yuan, F. Suarez-Ruiz, and I. M. Chen, "A telemanipulation-based human-robot collaboration method to teach aerospace masking skills," *IEEE Trans. Ind. Informat.*, vol. 16, no. 5, pp. 3076–3084, May 2020.

[5] D. F. Paez Granados, B. A. Yamamoto, H. Kamide, J. Kinugawa, and K. Kosuge, "Dance teaching by a robot: Combining cognitive and physical human–robot interaction for supporting the skill learning process," *IEEE Robot. Autom. Lett.*, vol. 2, no. 3, pp. 1452–1459, Jul. 2017.

[6] Z. Pang, G. Yang, R. Khedri, and Y. Zhang, "Introduction to the special section: Convergence of automation technology, biomedical engineering, and health informatics toward the Healthcare 4.0," *IEEE Rev. Biomed. Eng.*, vol. 11, pp. 249–259, Jul. 2018.

[7] M. Althoff, A. Giusti, S. B. Liu, and A. Pereira, "Effortless creation of safe robots from modules through self-programming and self-verification," *Sci. Robot.*, vol. 4, no. 31, Jun. 2019, Art. no. eaaw1924.

[8] S. Robla-Gomez, V. M. Becerra, J. R. Llata, E. Gonzalez-Sarabia, C. Torre-Ferrero, and J. Perez-Oria, "Working together: A review on safe human-robot collaboration in industrial environments," *IEEE Access*, vol. 5, pp. 26754–26773, Nov. 2017.

[9] G. Yang, G. Pang, Z. Pang, Y. Gu, M. Mantysalo, and H. Yang, "Non-invasive flexible and stretchable wearable sensors with nano-based enhancement for chronic disease care," *IEEE Rev. Biomed. Eng.*, vol. 12, pp. 34–71, Dec. 2018.

[10] V. Villani, F. Pini, F. Leali, and C. Secchi, "Survey on human–robot collaboration in industrial settings: Safety, intuitive interfaces and applications," *Mechatronics*, vol. 55, pp. 248–266, Nov. 2018.

[11] P. Aivaliotis, S. Aivaliotis, C. Gkournelos, K. Kokkalis, G. Michalos, and S. Makris, "Power and force limiting on industrial robots for human-robot collaboration," *Robot Comput. Integr. Manuf.*, vol. 59, pp. 346–360, Oct. 2019.

[12] G. Michalos, S. Makris, P. Tsarouchi, T. Guasch, D. Kontovrakis, and G. Chryssolouris, "Design considerations for safe human-robot collaborative workplaces," *Procedia CIRP*, vol. 37, pp. 248–253, Oct. 2015.

[13] P. Tsarouchi, S. Makris, and G. Chryssolouris, "Human-robot interaction review and challenges on task planning and programming," *Int. J. Comput. Integr. Manuf.*, vol. 29, no. 8, pp. 916–931, Feb. 2016.

[14] Y. Fei and H. Xu, "Modeling and motion control of a soft robot," *IEEE Trans. Ind. Electron.*, vol. 64, no. 2, pp. 1737–1742, Feb. 2017.

[15] L. Cao and W. J. Zhang, "Integrated design of compliant mechanisms and embedded rotary actuators and bending actuators for motion generation," presented at *ASME 2016 Int. Des. Eng. Techn. Conf. Comput. Inf. Eng. Conf.*, Charlotte, NC, USA, Aug. 21–24, 2016, Paper no. V05AT07A001

[16] H. M. Le, T. N. Do, L. Cao, and S. J. Phee, "Towards active variable stiffness manipulators for surgical robots," in *Proc. IEEE Int. Conf. Robot. Autom.*, 2017, pp. 1766–1771.

[17] H. M. Le, L. Cao, T. N. Do, and S. J. Phee, "Design and modelling of a variable stiffness manipulator for surgical robots," *Mechatronics*, vol. 53, pp. 109–123, Aug. 2018.

[18] S. Tsuji and T. Kohama, "Proximity skin sensor using time-of-flight sensor for human collaborative robot," *IEEE Sens. J.*, vol. 19, no. 14, pp. 5859–5864, Mar. 2019.

[19] D. Hughes, J. Lammie, and N. Correll, "A robotic skin for collision avoidance and affective touch recognition," *IEEE Robot. Autom. Lett.*, vol. 3, no. 3, pp. 1386–1393, Jul. 2018.

[20] T. Matsuno, Z. Wang, K. Althoefer, and S. Hirai, "Adaptive update of reference capacitances in conductive fabric based robotic skin," *IEEE Robot. Autom. Lett.*, vol. 4, no. 2, pp. 2212–2219, Apr. 2019.

[21] J. Yi and Y. L. Park, "Soft inflatable robotic sleeves for actuation and shock absorption," in *Proc. IEEE Int. Conf. Ubiquitous Robots*, 2018, pp. 208–208.

[22] P. Ohta *et al.*, "Design of a lightweight soft robotic arm using pneumatic artificial muscles and inflatable sleeves," *Softw. Robot.*, vol. 5, no. 2, pp. 204–215, Apr. 2018.

[23] R. Qi, A. Khajepour, W. W. Melek, T. L. Lam, and Y. Xu, "Design, kinematics, and control of a multijoint soft inflatable arm for human-safe interaction," *IEEE Trans. Robot.*, vol. 33, no. 3, pp. 594–609, Jun. 2017.

[24] W. W. Lee *et al.*, "A neuro-inspired artificial peripheral nervous system for scalable electronic skins," *Sci. Robot.*, vol. 4, no. 32, Jul. 2019, Art. no. eaax2198.

[25] T. Kim, S. J. Yoon, and Y.-L. Park, "Soft inflatable sensing modules for safe and interactive robots," *IEEE Robot. Autom. Lett.*, vol. 3, no. 4, pp. 3216–3223, Oct. 2018.
[26] T. Kim, J. Park, S. J. Yoon, D. H. Kong, H. Park, and Y. Park, "Design of a lightweight inflatable sensing sleeve for increased adaptability and safety of legged robots," in *Proc. IEEE Int. Conf. Softw. Robot.*, 2019, pp. 257–264.
[27] S. Papanastasiou *et al.*, "Towards seamless human robot collaboration: Integrating multimodal interaction," *Int. J. Adv. Manuf. Technol.*, to be published, doi: 10.1007/s00170-019-03790-3.
[28] Bluedanuberobotics.com, "AIRSKIN MODULE PADS," *Blue Danube Robotics*, 2018. [Online]. Available: https://www.bluedanuberobotics.com/wp-content/uploads/2019/05/AIRSKIN_ModulPads_201905.pdf. Accessed on: Nov. 12, 2019.
[29] Fogale-robotics.com, "Sensitive surfaces," *FOGALE Robot.*, 2019. [Online]. Available: https://www.fogale-robotics.com/pdf/Sensitive_surfaces.pdf. Accessed on: Nov. 12, 2019.
[30] M. Fritzsche, N. Elkmann, and E. Schulenburg, "Tactile sensing: A key technology for safe physical human robot interaction," in *Proc. ACM/IEEE Hum.-Robot Interact.*, 2011, pp. 139–140.
[31] J. J. Park, S. Haddadin, J. B. Song, and A. Albu-Schaffer, "Designing optimally safe robot surface properties for minimizing the stress characteristics of human-robot collisions," in *Proc. IEEE Int. Conf. Robot. Autom.*, 2011, pp. 5413–5420.
[32] ABB Robotics, "YuMi–IRB 14000," Nov. 2018. [Online]. Available: https://new.abb.com/products/robotics/industrial-robots/irb-14000-yumi/irb-14000-yumi-data
[33] Y. Huang, S. Li, S. Li, and Y. Ke, "Design and implementation of dual-arm robot with homogeneous compliant joint," in *Proc. Int. Conf. Intell. Hum.-Mach. Syst. Cybern.*, 2017, vol. 2, pp. 265–270.
[34] Y. She, H.-J. Su, D. Meng, S. Song, and J. Wang, "Design and modeling of a compliant link for inherently safe corobots," *J. Mech. Robot.*, vol. 10, no. 1, Dec. 2017, Art. no. 011001.
[35] Y. She, H. J. Su, C. Lai, and D. S. Meng, "Design and prototype of a tunable stiffness arm for safe human-robot interaction," in *Proc. ASME Int. Des. Eng. Tech. Conf. Comput. Inf. Eng. Conf.*, Aug. 2016, vol. 5b, Art. no. V05BT07A063.
[36] M. J. Rosenstrauch and J. Kruger, "Safe human-robot-collaboration-introduction and experiment using ISO/TS 15066," in *Proc. Int. Conf. Control Autom. Robot.*, 2017, pp. 740–744.
[37] D. G. Unfallversicherung, "BG/BGIA risk assessment recommendations according to machinery directive: Design of workplaces with collaborative robots," 2009. [Online]. Available: https://www.dira.dk/media/66056/bg-bgia_risk_assessment_recommendations_according_to_machinery_directive.pdf. Accessed on: Nov. 23, 2019.
[38] M. Melia *et al.*, "Pressure pain thresholds: Subject factors and the meaning of peak pressures," *Eur. J. Pain*, vol. 23, no. 1, pp. 167–182, Jan. 2019.
[39] R. Weitschat, J. Vogel, S. Lantermann, and H. Höppner, "End-effector airbags to accelerate human-robot collaboration," in *Proc. IEEE Int. Conf. Robot. Autom.*, 2017, pp. 2279–2284.
[40] X. Wu, Y. Han, X. Zhang, Z. Zhou, and C. Lu, "Large-area compliant, low-cost, and versatile pressure-sensing platform based on microcrack-designed carbon black@ polyurethane sponge for human-machine interfacing," *Adv. Funct. Mater.*, vol. 26, no. 34, pp. 6246–6256, Jun. 2016.
[41] H. Dal and M. Kaliske, "Bergstrom-Boyce model for nonlinear finite rubber viscoelasticity: Theoretical aspects and algorithmic treatment for the FE method," *Comput. Mech.*, vol. 44, no. 6, pp. 809–823, Nov. 2009.
[42] G. Pang, J. Deng, F. Wang, J. Zhang, Z. Pang, and G. Yang, "Development of flexible robot skin for safe and natural human-robot collaboration," *Micromachines*, vol. 9, no. 11, Nov. 2018, Art. no. 576.
[43] R. K. W. Vithanage, C. S. Harrison, and A. K. M. De Silva, "Autonomous rolling-stock coupler inspection using industrial robots," *Robot Comput. Integr. Manuf.*, vol. 59, pp. 82–91, Oct. 2019.
[44] X. G. Li, L. Cao, A. M. H. Tiong, P. T. Phan, and S. J. Phee, "Distal-end force prediction of tendon-sheath mechanisms for flexible endoscopic surgical robots using deep learning," *Mech. Mach. Theory*, vol. 134, pp. 323–337, Apr. 2019.
[45] P. Polygerinos *et al.*, "Soft robotics: Review of fluid-driven intrinsically soft devices; manufacturing, sensing, control, and applications in human-robot interaction," *Adv. Eng. Mater.*, vol. 19, no. 12, May 2017, Art. no. 1700016.
[46] Q. Chen, J. Zhao, J. Ren, L. Rong, P. F. Cao, and R. C. Advincula, "3D printed multifunctional, hyperelastic silicone rubber foam," *Adv. Funct. Mater.*, vol. 29, no. 23, 2019, Art. no. 1900469.
[47] Y. Huang *et al.*, "Performance evaluation of a foot interface to operate a robot arm," *IEEE Robot. Autom. Lett.*, vol. 4, no. 4, pp. 3302–3309, Jul. 2019.
[48] Y. Huang, E. Burdet, L. Cao, P. T. Phan, A. H. T. Meng, and L. Phee, "A subject-specific four-degree-of-freedom foot interface to control a surgical robot," *IEEE/ASME Trans. Mechatronics*, to be published.
[49] G. Cannata, S. Denei, and F. Mastrogiovanni, "Towards automated self-calibration of robot skin," in *Proc. IEEE Int. Conf. Robot. Autom.*, 2010, pp. 4849–4854.
[50] S. Youssefi, S. Denei, F. Mastrogiovanni, and G. Cannata, "A real-time data acquisition and processing framework for large-scale robot skin," *Robot Auton. Syst.*, vol. 68, pp. 86–103, Jun. 2015.

Gaoyang Pang (Student Member, IEEE) received the B.Eng. degree in mechanical design, manufacturing and automation from the College of Mechanical and Vehicle Engineering, Hunan University, Changsha, China, in 2017. He is currently working toward the M.Sc. degree in mechatronics engineering with the school of Mechanical Engineering, Zhejiang University, Hangzhou, China.

His research interests include flexible sensing electronics, wearable sensors using inkjet printing technology, and safe human–robot collaboration strategies.

Geng Yang (Member, IEEE) received the B.Eng. degree in instrument science and engineering and the M.Sc. degree in instrument science and technology from the College of Biomedical Engineering and Instrument Science, Zhejiang University (ZJU), Hangzhou, China, in 2003 and 2006, respectively, and the Ph.D. degree in electronic and computer systems from the Department of Electronic and Computer Systems, the Royal Institute of Technology (KTH), Stockholm, Sweden, in 2013.

From 2013 to 2015, he was a Postdoctoral Researcher with iPack VINN Excellence Center, the School of Information and Communication Technology, KTH. He is currently a Research Professor with the School of Mechanical Engineering, ZJU. He developed low power, low noise bio-electric state of charge (SoC) sensors for m-health. His research interests include flexible and stretchable electronics, mixed-mode integrated circuit (IC) design, low-power biomedical microsystem, wearable bio-devices, human–computer interface, human–robot interaction, intelligent sensors, and Internet-of-Things for healthcare.

Wenzheng Heng is currently working toward the B.E. degree in mechatronics engineering with the School of Mechanical Engineering, Zhejiang University, Hangzhou, China.

His research interests include flexible electronics for medical and robotics applications, integration of flexible sensing and soft actuating, and soft robots.

Zhiqiu Ye received the B.S. degree in mechanical design, manufacturing and automation from the College of Mechanical and Electrical Engineering, Central South University, Changsha, China, in 2019. He is currently working towards the Ph.D. degree in mechatronics engineering with the School of Mechanical Engineering, Zhejiang University, Hangzhou, China.

His research interests include flexible sensors for human–robot interaction and the applications of inkjet printing technology in flexible electronics.

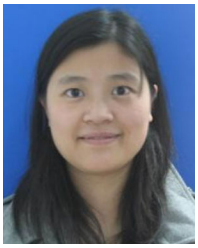

Xiaoyan Huang (Member, IEEE) received the B.E. degree in instrument science and engineering from Zhejiang University, Hangzhou, China, in 2003, and received the Ph.D. degree in electrical machines and drives from the University of Nottingham, Nottingham, U.K., in 2008.

From 2008 to 2009, she was a Research Fellow with the University of Nottingham. She is currently a Professor with the College of Electrical Engineering, Zhejiang University, where she is working on electrical machines and drives. Her research interests are permanent magnet machines and drives for transportation vehicles.

Hua-Yong Yang received the B.S. degree in mechanical engineering from the Huazhong University of Science and Technology, Wuhan, China, in 1982, and the Ph.D. degree in mechanical engineering from the University of Bath, Bath, U.K., in 1988.

Since 1989, he has been with Zhejiang University, Hangzhou, China as a Postdoctoral Researcher. He is currently a Professor and the Director of the State Key Laboratory of Fluid Power and Mechatronic Systems and the School of Mechanical Engineering. He has authored and coauthored three academic books, 76 Science Citation Index (SCI) papers, 210 Engineering Index (EI) papers, and has 169 invention patents. His research interests are in motion control and energy saving of mechatronic systems, development of fluid power component and system, integration of electro-hydraulic system, and engineering application.

Dr. Yang was the recipient of the first class of the National Scientific and Technological Progress Award, the National Outstanding Researcher of the Natural Science Foundation of China, and three Ministerial or Provincial Scientific and Technological Progress Prizes. He is an Academician of the Chinese Academy of Engineering.

Zhibo Pang (Senior Member, IEEE) received the B.Eng. degree in electronic engineering from Zhejiang University, Hangzhou, China, in 2002, the MBA degree in innovation and growth from University of Turku, Turku, Finland in 2012, and the Ph.D. degree in electronic and computer systems from the Royal Institute of Technology (KTH), Stockholm, Sweden, in 2013.

He is currently a Principal Scientist in Wireless Communications with ABB Corporate Research, Västerås, Sweden. Before joined ABB, he was Co-Founder and Chief Technical Officer of startups, such as Ambigua Medito AB.

Dr. Pang was the recipient of the "2016 Inventor of the Year Award" by ABB Corporate Research, Sweden. He is a Co-Chair of the Technical Committee on Industrial Informatics. He is an Associate Editor of the IEEE TRANSACTIONS ON INDUSTRIAL INFORMATICS and IEEE JOURNAL OF BIOMEDICAL AND HEALTH INFORMATICS and a Guest Editor of the PROCEEDINGS OF THE IEEE, IEEE INTERNET OF THINGS JOURNAL, and IEEE REVIEWS IN BIOMEDICAL ENGINEERING.